Supporting information

Direct Growth of 2D Nickel Hydroxide Nanosheets Intercalated with Polyoxovanadate Anions as a Binder-Free Supercapacitor Electrode

Jayavant L. Gunjakar,[a,c] Akbar I. Inamdar,[a] Bo Hou,[b] Seung Nam Cha,[b] S. M. Pawar,[a] Abu Talha A. A.,[a] Harish S. Chavan,[a] Jongmin Kim,[a] Sangeun Cho,[a] Seongwoo Lee,[a] Yongcheol Jo,[a] Hyungsang Kim[a] and Hyunsik Im[a*]

[a.] *Division of Physics and Semiconductor Science, Dongguk University, Seoul 04620, South Korea. E-mail: hyunsik7@dongguk.edu*
[b.] *Department of Engineering Science, University of Oxford, Parks Road, OX1 3PJ, UK*
[c.] *D. Y. Patil Education Society, Kolhapur, India*

Electronic Supplementary Information (ESI) available: [EDS–elemental maps, EDS spectrum, Micro-Raman, Capacity retention]. See DOI: 10.1039/x0xx00000x

S1) Reaction Mechanism for the deposition of LNHV.

The CSD of thin films is a controlled precipitation technique that is basedon the principle of solid phase formation during the transformation from a supersaturated state to a saturated state.[1] During the deposition of LNHV thin films, a supersaturated aqueous solution of a hexamine $Ni(NH_3)_4^{+2}$ complex and sodium orthovanadate (Na_3VO_4) transforms into a saturated state via the gradual evaporation of ammonia (NH_3).

The typical CDS process involves following stepwise reactions

1) The dissolution of $NiCl_2$ in water gives the octahedral hexa-aqua nickel (II) complex ion, as follows:[2]

$$xNiCl_2 + xyH_2O \rightarrow x[Ni(H_2O)_y]^{2+}_{(aq)} + 2x(Cl_2)^- \quad (1)$$

2) The reaction of hexa-aqua nickel (II) complex ionwith liquid NH_3 gives a greenish precipitate of the hydrated $Ni(OH)_2$ forms via the hydroxide group-derived *olation* process of the stepwise replacement of the H_2O ligand molecules, as follows:

$$x[Ni(H_2O)_p]^{2+} + y(OH)^{2-} \leftrightarrow [Ni_x(OH)_y(H_2O)_{xp-y}]^{(2x-y)+} at\ pH < 9,$$

$$x[Ni(H_2O)_p]^{2+} + y(OH)^{2-} \leftrightarrow Ni_x(OH)_{2n}(s) + (xp-y)H^+ at\ pH > 9 \quad (2)$$

3) Further excess addition of NH_3transforms the green precipitate of $Ni(OH)_2$ into a clear blue solution of the hexamine nickel complex ($Ni(NH_3)_q^{2+}$), where q is the coordination number, and 6 is the most stable for Ni^{2+}.[3,4]The formation of the hexamine nickel complex prevents a spontaneous precipitation, leading to the formation of a supersaturated solution, as follows:

$$Ni_x(OH)_{2x} + qNH_4^+ + q(OH)^- \leftrightarrow Ni_x(NH_3)_q^{2x+} + qH_2O + 2x(OH)^- at\ pH > 12 \quad (3)$$

On the other hand hydrolysis of vanadium precursor produces a large variety of POV anions with diverse structures, e.g., chain metavanadates $[VO_3^-]_n$, layered oxides $[V_2O_5]$, and compact polyanions $[V_{10}O_{28}]^{6-}$. The structure of these polyoxovanadium ions are solely depends on the concentration and pH.[2,5,6] Pentavalent V^{5+} ions induce the $[V(OH_2)_6]^{5+}$ solvated species that are formed in aqueous solution and are surrounded by dipolar H_2O molecules. Considering strong polarizing power and Lewis properties associated with V^{5+} and H_2O, respectively, some of the electrons transfer from the $3a_1$ orbital of the water

molecule to the empty 3d orbitals in the V^{5+} leading spontaneous acidification and deprotonation of the H_2O molecules are represented by the following hydrolysis reaction:

$$[V(OH_2)_6]^{5+} + hH_2O \rightarrow [V(OH)_h(OH_2)_{6-h}]^{(5-h)+} + hH_3O^+ \quad (4)$$

In above reaction the hydrolysis ratio, h, increases with the pH, leading to the formation of aquo, hydroxo, or oxo species. In the beginning, the pH of the aqueous Na_3VO_4 solution is above 12, and the monomeric, tetrahedral oxo-anionic VO_4^{3-} speciesare produced. The structure of polyoxovandium anions and stability are reported previously.[5,6]A CSD bath for LNHV is made up of thesupersaturated hexaminenickel complex solution and subsequent addition of a monomeric orthovanadate (VO_4^{3-}). The addition of monomeric orthovanadate (VO_4^{3-}) to supersaturated hexaminenickel complex solution leads to a transparent, supersaturated CSD bath with a slight increase in the pH depending on the amount of the VO_4^{3-} precursor, and the colour changes from transparent blue to dark cyan. The CSD bath is maintained at an elevated temperature (~50 ºC) with the vertically immersed substrates. Consequently, the ionic product exceeds its solubility product via the release of H_2O and NH_3. The CSD bath gradually becomes saturated, and precipitation occurs through the heterogeneous growth of $Ni(OH)_2$ that has been pillared with the POV anions on the substrate and homogeneous growth in the solution phase.

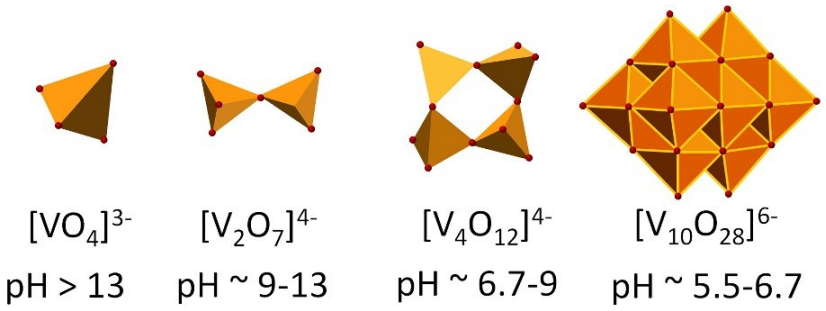

Fig. S1. Structural of polyoxovanadate in H_2O and their stabilization pH range. (Refs. 5,6)

The type of the intercalated species can be predicted by observing the change in the pH. Various possible structural forms of polyoxovanadium present in the solution at the used precursor concentration in CSD are represented in fig. S1, however only $[V_2O_7]^{4-}$ and $[V_4O_{12}]^{4-}$ are the polyoxovanadium anions predominant at the hydrolysis reaction pH of CSD. As the precipitation process proceeds, the pH changes

from 12.5 to ~ 7. As the pH gradually decreases to ~9, condensation occurs due to the continuous deprotonation that leads to the transformation of the VO_4^{3-} species into dimeric pyrovanadates $[V_2O_7]^{4-}$. In the pH range from ~7 to 9, a more condensed, cyclic-metavanadate $[V_4O_{12}]^{4-}$ can form.[6]Consequently,the intercalated POV anions are most likely $[V_2O_7]^{4-}$ or $[V_4O_{12}]^{4-}$.

S2) BET analysis for LNHV-1 nanohybrids

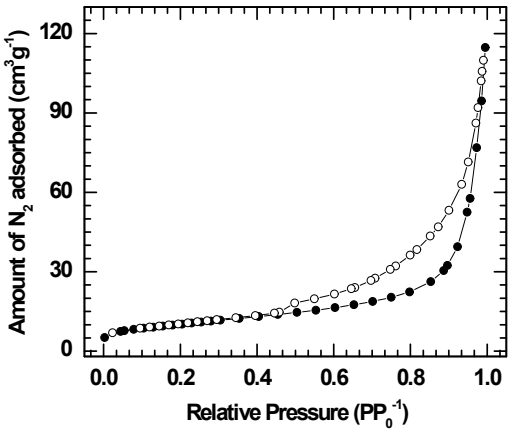

Fig. S2. N_2 adsorption-desorption isotherm for LNHV-1 nanohybrids.

The evolution of the pore structure and surface area of the LNHV-1 nanohybrid is examined using N_2 adsorption-desorption isotherm measurements. As shown in Fig. S2, the LNHV-1 nanohybrid exhibits significant N_2 adsorption in the low-pressure region ($pp_0^{-1} < 0.4$) with distinct hysteresis in the high-pressure region ($pp_0^{-1} > 0.45$) representing the incorporation of mesopores in the materials. Based on the IUPAC classification, the present isotherms showing sloping adsorption and desorption branches covering a large range of pp_0^{-1} with hysteresis behavior are classified as Brunauer-Deming-Deming-Teller (BDDT)-type IV shapes and a H3-type hysteresis loop. The present N_2 adsorption-desorption isotherm behavior is characteristic of a well-ordered mesoporous material with high adsorption energy and slit-shaped pores. The observed adsorption-desorption isotherm behavior is rather similar to the LDH intercalated with polyoxomatalate anions synthesized by the exfoliation-reassembling and ion exchange route. The LNHV-1 nanohybrid demonstrated an expanded surface area of 36 m^2g^{-1} calculated using the Brunauer-Emmett-Teller (BET) equation. BET analysis highlights the usefulness of the chemical

solution deposition method for the deposition of $Ni(OH)_2$−POV nanohybrids with an expanded surface area.

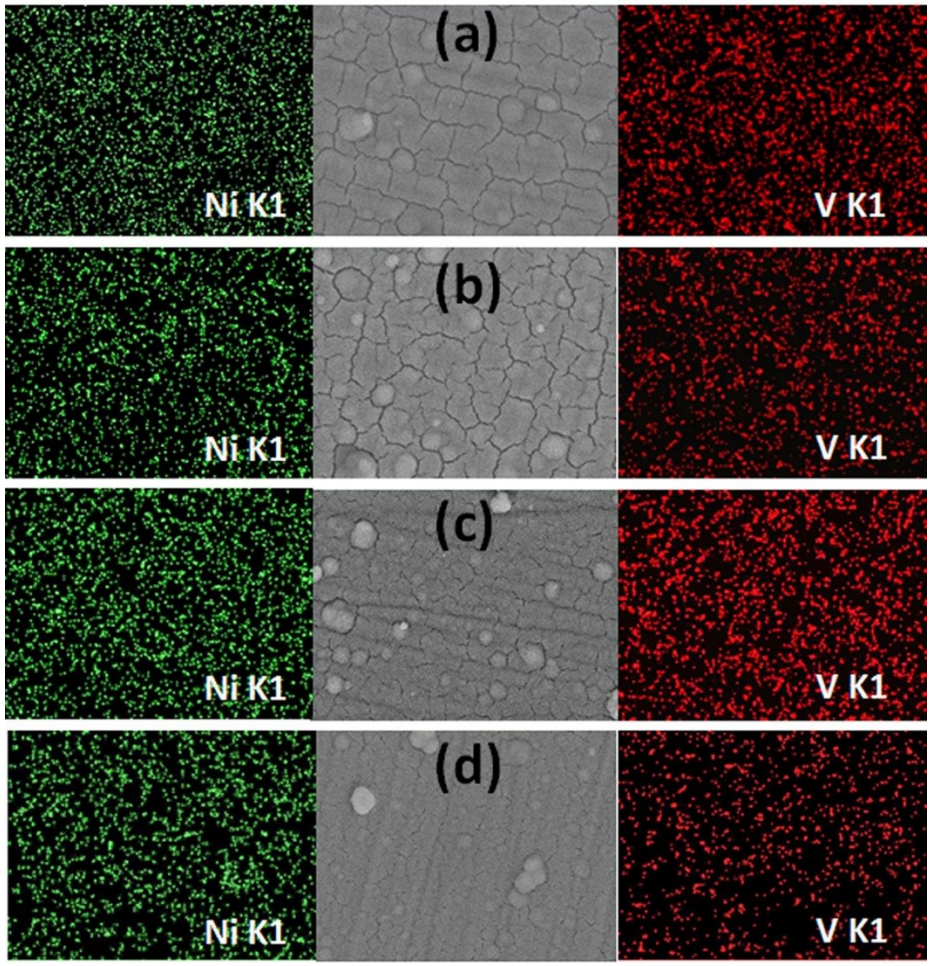

Fig. S3. EDS−elemental maps of the(a) LNHV-2, (b) LNHV-1.5, (c) LNHV-1, and (d) LNHV-0.5.

The spatial distributions of component elements in the $Ni(OH)_2$−POV thin films are probed with EDS−elemental mapping analysis. As shown in fig. S3, EDS−elemental maps demonstrating uniform distribution of all component elements, i.e. nickel, vanadium, and oxygen in entire parts of the $Ni(OH)_2$−POV thin films, clearly demonstrating the homogeneous intercalation of polyoxomatalate anions without any phase separation.

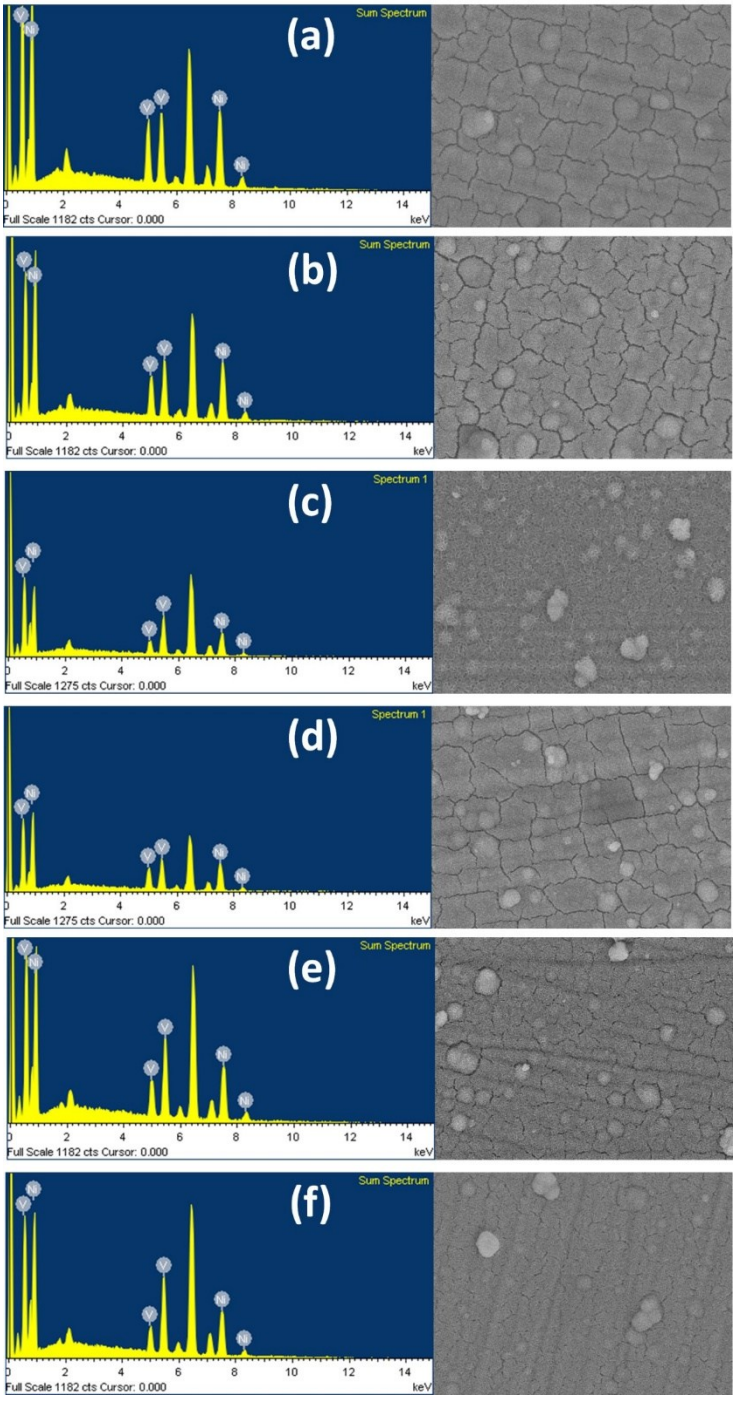

Fig. S4. Energy dispersive X-ray spectroscopy EDS spectrum of (a) LNHV-3, (b) LNHV-2.5, (c) LNHV-2, (d) LNHV-1.5, (e) LNHV-1, and (f) LNHV-0.5.

Fig. S4 shows the EDS spectrum of the $Ni(OH)_2$−POV thin films deposited at various Ni:V precursor ration. All of the EDS spectra showed the presence of nickel vanadium and oxygen elements in $Ni(OH)_2$−POV thin films. The elemental analysis clearly indicating final Ni:V ratio in $Ni(OH)_2$−POV thin films is decrease from 4.24 to 3.25 with initial Ni:V ratio. Beyond this point, the final Ni:V ratio appears to be constant with further increase of initial Ni:V ratio. Due to rapid fall of pH for further initial Ni:V reactant ratio, the deposited $Ni(OH)_2$−POV thin films become powdery and less adherent beyond the ratio 3 (The ratio of 3 corresponds to a fall of pH from 13 to 7), reflecting uncontrolled precipitation of material in the bulk form. Consequently the vanadium percentage in the $Ni(OH)_2$−POV thin films increase at higher initial Ni:V reactant ratio with more condense isopolyoxomatalate. $[V_4O_{12}]^{4-}$. In the low initial Ni:V reactant ratio <0.5, (The ratio of 0.5 corresponds to a fall of pH from 13 to 9) the precipitation of $Ni(OH)_2$−POV is too slow, thus leading to the formation of ultrathin $Ni(OH)_2$−POVfilms. Subsequently the vanadium percentage in the $Ni(OH)_2$−POV thin films decrease at lower initial Ni:V reactant ratio with less condense isopolyoxomatalate $[V_2O_7]^{4-}$. In the intermediate ration of 0.5 to 3 the uniform and adherent $Ni(OH)_2$−POV thin films can be obtained with controlled POM content. Based on the chemical elemental analysis, the chemical composition of the $Ni(OH)_2$−POV thin films are determined to be $Ni(OH)_{1.68}{\cdot}0.08[V_4O_{12}]{\cdot}yH_2O$, $Ni(OH)_{1.69}{\cdot}0.077[V_4O_{12}]{\cdot}yH_2O$, $Ni(OH)_{1.71}{\cdot}0.072[V_4O_{12}]{\cdot}yH_2O$, $\{Ni(OH)_{1.73}{\cdot}0.0675[V_4O_{12}]{\cdot}yH_2O$,$Ni(OH)_{1.75}{\cdot}0.0625[V_4O_{12}]{\cdot}yH_2O$, $Ni(OH)_{1.77}{\cdot}0.0575[V_4O_{12}]{\cdot}yH_2O\}$ $Ni(OH)_{0.92}{\cdot}0.135[V_2O_7]{\cdot}yH_2O$, $Ni(OH)_1{\cdot}0.125[V_2O_7]{\cdot}yH_2O$, and $Ni(OH)_{1.08}{\cdot}0.115[V_2O_7]{\cdot}yH_2O$ for LNHV-3, LNHV-2.5, LNHV-2, LNHV-1.5, LNHV-1, and LNHV-0.5, respectively. This result clearly demonstrates the tunability of the chemical composition of the present $Ni(OH)_2$−POV thin films.

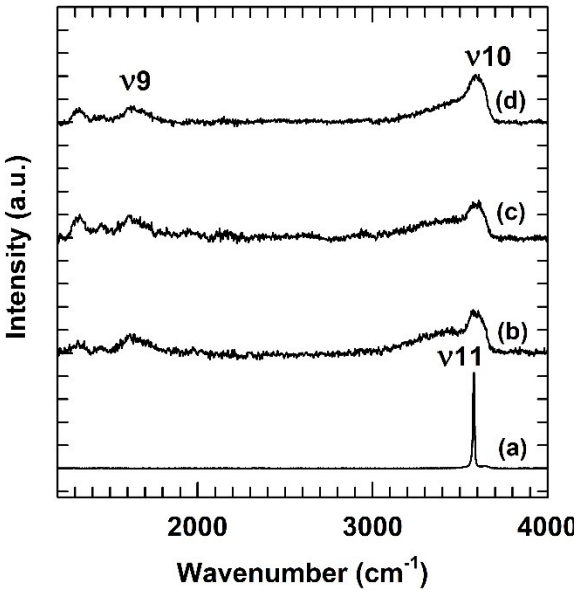

Fig. S5. Micro-Raman spectra of (a) LNHV-3,(b) LNHV-1.5, (c) LNHV-0.5, and (d) LNHV-0 thin films deposited on stainless steel.

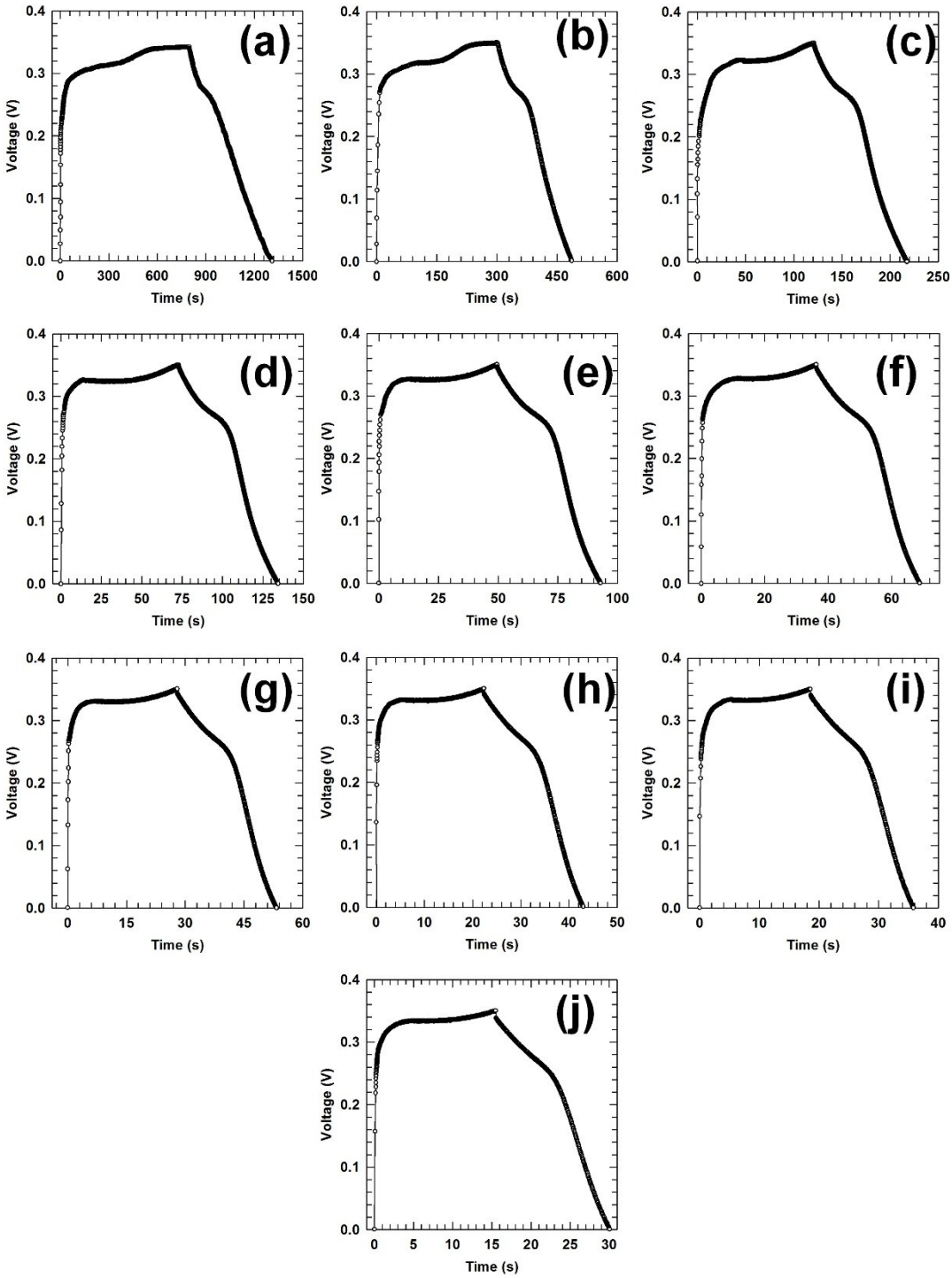

Fig. S6. Charge-discharge curves of LNHV-1 nanohybrid at (a) 1, (b) 2, (c) 3, (d) 4, (e) 5, (f) 6, (g) 7, (h) 8, (i) 9 and (j) 10 Ag^{-1}.

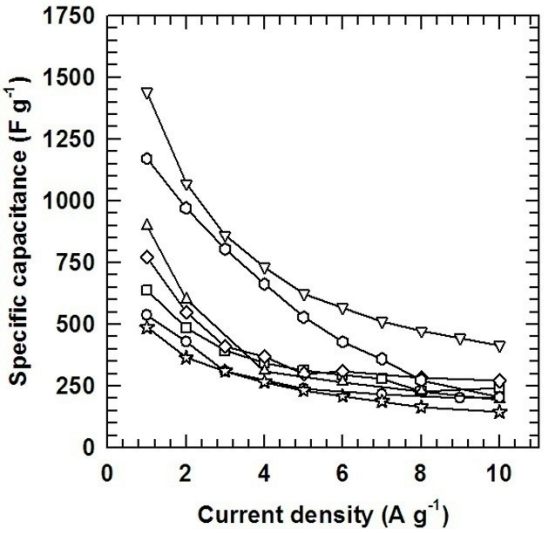

Fig. S7. Comparison of the variations of the specific capacitance of $Ni(OH)_2$−POV thin films at increasing current density;(circle) LNHV-3, (square) LNHV-2.5, (diamond) LNHV-2, (triangle-up) LNHV-1.5, (triangle-down) LNHV-1, (hex) LNHV-0.5, and (star) LNHV-0.

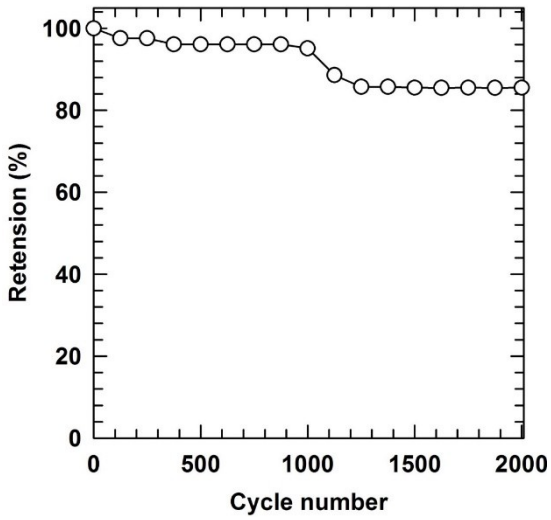

Fig. S8. Retention of the specific capacitance of the **LNHV-1** at very high current density of 10 Ag^{-1}.

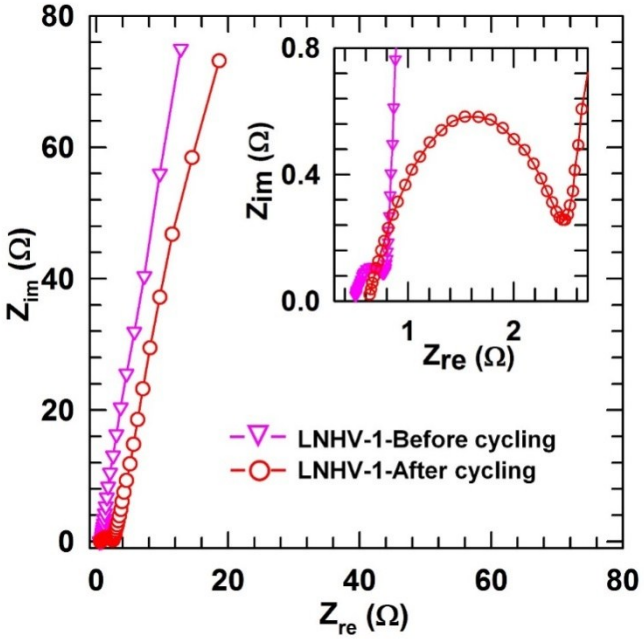

Fig. S9. Nyquist plots of the LNHV-1 thin film electrodes. (triangle-down) LNHV-1 before cycling and (circle) LNHV-1 after cycling test. The inset shows an enlarged view of the EIS spectra in the high frequency region.

Figure S9 shows the Nyquist plots for the LNHV-1 thin film electrode before and after cycling test. Both the test shows partially overlapping semicircles in the high frequency region. The presence of a semicircle is linked to the resistance of the electrolyte (R_e) and the charge transfer resistance (R_{ct}). LNHV-1 thin film electrode demonstrated the similar EIS characteristic before and after cycling with slight increase in starting point and diameter of semicircle. The observed increase is ascribed to the slight dissolution of electrode material and intercalation of electrolyte ions in the layered structure of LNHV-1 nanohybrid. It is observed that even after cycling LNHV-1 electrode demonstrated much smaller semicircle compared with the pristine $Ni(OH)_2$ electrode, which indicates the maintenance of improved charge transfer and the electrical conductivity of the LNHV-1 electrode after cycling. Furthermore the inclined lines in the low-frequency region correspond to the Warburg impedance, which is associated with the diffusion of the electrolyte ions into the bulk electrodes. Before and after cycling, LNHV-1 electrode demonstrated similar characteristics with much larger slope as compare to bare $Ni(OH)_2$ electrode (LNHV-0), which implies maintenance of lower resistance for the diffusion of the electrolyte ions throughout the electrode after cycling.

Table S10: Comparative supercapacitance performance of $Ni(OH)_2$ and its intercalative composite.

	Materials	Electrode Composition /Eectrolyte/Current collector	Maximum Specific Capacitance ($F\ g^{-1}$)	Stability retention (Cyclic number)	Ref.
1	Honeycomb-like β-$Ni(OH)_2$ thin films	β-$Ni(OH)_2$ thin films/2 M KOH/ stainless steel	398 (CV scan rate 5 mVs^{-1})		7
2	α-$Ni(OH)_2$ nanosheet based hierarchical microspheres (NBHMs) intercalated with Cl^- anions	NBHMs+vapor-grown carbon fiber as a conducting material + poly (vinylidene fluoride) (PVDF)/ 1 M KOH/ Ni-foam	1494 (1 Ag^{-1})	500	8
3	β-$Ni(OH)_2$ thin films	β-$Ni(OH)_2$ thin films/ 2M KOH/ stainless steel	468 (0.5 $mAcm^{-1}$)	1000	9
4	β-$Ni(OH)_2$ thin films by SILAR method	β-$Ni(OH)_2$ thin films/ 2M KOH/ stainless steel	350 (CV scan rate 20 mVs^{-1})		10
5	β-$Ni(OH)_2$ /γ-NiOOH composite film	β-$Ni(OH)_2$ /γ-NiOOH composite film/ 1 M KOH/ Ni-foam	1420 (2 Ag^{-1})	1000	11
6	β-$Ni(OH)_2$ nanoparticles	β-$Ni(OH)_2$ nanoparticles/1 M KOH/ stainless steel	715.3 (0.5 Ag^{-1})		12
7	$Ni(OH)_2$ mixed phase	$Ni(OH)_2$ mixed phase+20 wt% carbon black + 5 wt% polytetrafluoroethylene (PTFE)/ 1 M KOH/ Ni-foam	755 (1 Ag^{-1})	500	13
8	Ni foam decorated $Ni(OH)_2$ nanoflakes array	Ni foam decorated $Ni(OH)_2$ nanoflakes array/ 3 M KOH/ Ni-foam	1228 (5 Ag^{-1})	1000	14
9	$Ni(OH)_2$ glucose assisted solvothermal synthesis.	$Ni(OH)_2$ + conductive graphite +polyvinylidene difluoride (PVDF)/ 2 M KOH/ Ni-foam	1055 (1 Ag^{-1})	1000	15
10	Interstratified hybrids of α-hydroxides of nickel and cobalt	α-hydroxide of Ni and Co+graphite+binder PTFE/ 2 M KOH/ Ni-foam	990 (1 Ag^{-1})	600	16
11	MnO_2-pillared NiFe-LDH	MnO_2-pillared NiFe-LDH+ acetylene black + polyvinylidene fluoride/ 1 M Na2SO4/ Ni-mesh	190 (CV scan rate 5 mVs^{-1})		17
12	$Ni(OH)_2$ intercalated with polyoxovanadate anions ($Ni(OH)_2$−POV)	$Ni(OH)_2$−POV thin films/ 2 M KOH/ stainless steel	1440 (1 Ag-1)	2000	Present work

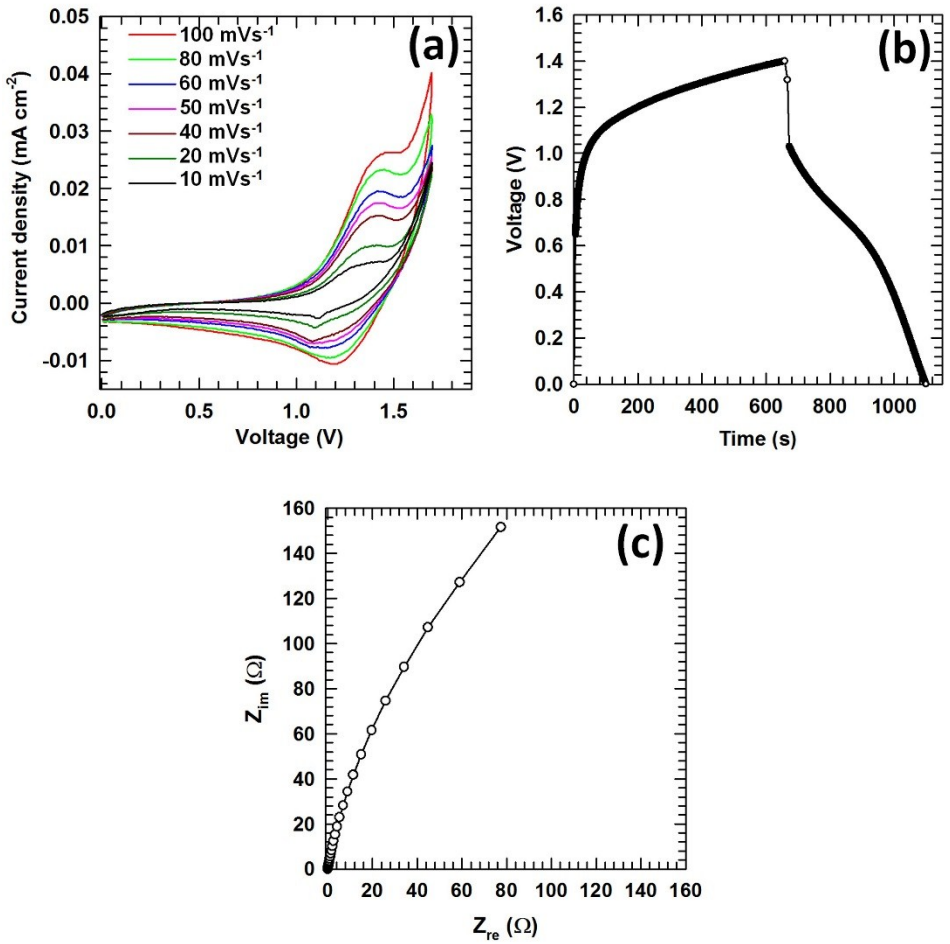

Fig. S11. (a) CV curves of the symmetric $Ni(OH)_2$−POV (LHNV-1) thin film supercapacitor at various scan rates. (b) GCD curve of the symmetric $Ni(OH)_2$−POV (LHNV-1) thin film supercapacitor at 1 Ag^{-1}. (c) Nyquist plot of the symmetric $Ni(OH)_2$−POV (LHNV-1) thin film supercapacitor.

We tested supercapacitance performance of the LNHV-1 nanohybrids for the two electrode configuration. The LNHV-1 nanohybrid electrodes are used as a positive and negative electrode for symmetric devise configuration. The LNHV-1 nanohybrids demonstrated promising supercapacitive activity with a wide operating potential window of 0 to 1.7 V and specific capacitance of 285.7 Fg^{-1}.

References

1. G. Hodes, *Chemical solution deposition of semiconductor films*. Marcel Dekker, New York, 2003; p. 2.

2. C. F. Baes and R. E. Mesmer, In *The hydrolysis of cations*. Wiley, New York,1976; p. 241.

3. Y. G., Li, B.Tan and Y. Wu, *Chem. Mater.* 2008, **20**, 567-576.

4. I. Ichinose, K. Kurashima, and T. Kunitake, *J. Am. Chem. Soc.* 2004, **126**, 7162-7163.

5. J. Livage, *Coordin. Chem. Rev.* 1998, **178**, 999-1018.

6. Y. Hayashi, *Coordin. Chem. Rev.*2011, **255**, 2270-2280.

7. U. M. Patil, K. V. Gurav, V. J. Fulari, C. D. Lokhande, and O. S. Joo, J. Power Sources 2009, 188, 338–342.

8. J. W. Lee, J. M. Ko, and J. D. Kim, J. Phys. Chem. C 2011, 115, 19445–19454.

9. D. P. Dubal, V. J. Fulari, and C. D. Lokhande, Micropor. Mesopor. Mater. 2012, 151, 511–516.

10. S. B. Kulkarni, V. S. Jamadade, D. S. Dhawale, and C. D. Lokhande. Appl. Surf. Sci. 2009, 255, 8390–8394.

11. Y. F. Yuan, X. H. Xia, J. B. Wu, J. L. Yang, Y. B. Chen, and S. Y. Guo, Electrochim. Acta 2011, 56, 2627–2632.

12. M. Aghazadeh, A. N. Golikand, and M. Ghaemi, Int J Hydrogen Energy 2011, 36, 8674-8679.

13. P. Lu, F. Liua, D. Xue, H. Yang, and Y. Liu, Electrochim. Acta 2012, 78, 1-10.

14. B. Hu, X. Qin, A. M. Asiri, K. A. Alamry, A. O. Al-Youbi, and X. Sun, Electrochim. Acta 2013, 107, 339– 342.

15. G. Lee, C. V. Varanasi, and J. Liu, Nanoscale, 2015, 7, 3181–3188.

16. M. Sebastian, C. Nethravathi, and M. Rajamathi, Mater. Res. Bul. 2013, 48, 2715–2719.

17. H. Li, G. Zhu, Z. Yang, Z. Wang, and Z. Liu, J. Colloid Interface Sci. 2010, 345, 228–233.